Aeroelastic Analysis by Coupled Non-linear Time Domain Simulation

Jens Neumann, Jens Nitzsche, Ralph Voss
Deutsches Zentrum für Luft- und Raumfahrt e.V. in der Helmholtz-Gemeinschaft
German Aerospace Center, Member of the Helmholtz Association
Institute of Aeroelasticity
Bunsenstrasse 10, D-37073 Göttingen

jens.neumann@dlr.de; jens.nitzsche@dlr.de; ralph.voss@dlr.de

ABSTRACT

For an accurate prediction of the steady and unsteady behaviour of an aircraft it is necessary to take into account the deformations of the structure due to the aerodynamic loads and thus the changing of the aerodynamic surface. This is of special importance for transonic and viscous flows, which are very sensitive to small contour changes. The appearance of strong shocks, shock boundary-layer interaction and shock induced flow separation may significantly affect the flutter boundary of an aircraft and cause limit cycle flutter oscillations of the structure. These effects can not be predicted by classical flutter stability computations and without adopting Computational Fluid Dynamics (CFD) codes. Non-linear aerodynamics and high fidelity structure models have to be taken into account within a high-precision fluid structure interaction simulation. In this paper some of the activities at the Institute of Aeroelasticity in the area of steady and unsteady fluid structure interaction will be presented. A process chain for both steady and unsteady aeroelastic applications has been developed in the last years, allowing the coupling between DLR's in-house CFD code TAU and the commercial FEM-based structural mechanics solver MSC.NASTRAN. Steady and unsteady applications are presented to demonstrate the suitability of the approach, including whole aircraft configurations and various windtunnel experiments. At first we are going to give an overview of the methods used inside the coupling procedure. For several experimental 2- and 3-dimensional test cases results will be presented. The predicted static aeroelastic behaviour of test configurations are in good agreement with windtunnel results. Obtained results for flutter simulations in the time domain demonstrate the superiority of coupled fluid-structure simulations compared to classical flutter calculations for viscous and transonic flows. The characteristic drop of the flutter boundary in transonic flow, the well-known "transonic dip" is well captured and limit cycle flutter is predicted. Finally, the paper discusses future developments necessary to further enhance the simulation capabilities for multidisciplinary simulation and optimization in the field of aeroelasticity.

1. INTRODUCTION

Aeroelastic simulation comprises the prediction of steady and unsteady aeroelastic phenomena, e.g. wing deformation, stability analysis (flutter, buffet) and dynamic response, e.g. gust loads. Furthermore analysis of large aircraft in cruise or maneuvering requires to take into account trim respectively large rigid body motions in the aeroelastic simulation.

Most standard aeroelastic analysis is performed in the frequency domain, which is justified as long as both aerodynamic and structural forces may be approximated to be linear with respect to size of structural deflections. In high-speed flight and in the case of large angles of attack aeroelastic effects can only be analyzed correctly using coupled high-fidelity models of structural dynamics (Finite Element Analysis) and of computational fluid dynamics (CFD). This higher level of structural and aerodynamic modeling is

especially required if in transonic and viscous or even separated flow complex shock motions, limit cycle oscillations (LCO) or large deflections occur. To be able to handle large scale, industrial configurations, the numerical models are usually set up in well-established and validated disciplinary codes. Static deflections and dynamic stability and response can then be simulated directly using co-simulation among the disciplinary codes.

At the DLR Institute of Aeroelasticity in addition to classical flutter analysis in sub- and transonic flows, increasing effort has been put on coupled non-linear simulations of various degrees of complexity during the last years. Examples of this recent work shown here, comprise the computation of static structural deflections of a trimmed aircraft, flutter boundaries and limit cycle oscillations (LCO) under transonic and separated flow conditions. This paper describes the approaches used for numerical simulation of elastic deformations, flutter stability and LCO oscillations, gives examples for numerical test cases as well as validations and comparisons with experimental data. The test data were obtained from transonic aeroelastic tests in different windtunnels by the institute, partly in cooperation with other DLR partners. Finally, some lessons learned for the selection of solution methods for various problems are given.

2. THE AERODYNAMIC SOLVER

For the results presented here the TAU code [8], [9] has been coupled with structural and flight mechanic solvers. It was applied for steady and unsteady computations on unstructured hybrid grids around different configurations. The DLR TAU flow simulation package comprises a finite-volume solver of the Reynolds-Averaged Navier-Stokes (RANS) equations, including several 1- and 2-equation turbulence models as well as LES- and DES models, on unstructured grids. Additionally the package includes a pre-processor, a grid adaptation module and a grid deformation module [7]. Different interfaces with structural analysis software allow coupled simulations of static and dynamic aeroelastic problems. The pre-processing module is used for constructing a dual grid of control volumes, from the initial grid which can be composed of tetrahedral, prismatic, hexahedral or pyramidal elements, and for partitioning of the grid for use of parallel computations. The dual grid contains information about metric data, boundary types and neighbouring domains. The CFD grids were generated adopting the commercial software Centaur [10].

For spatial discretization a centered scheme with scalar artificial dissipation is used combined with an explicit 3-stage Runge-Kutta scheme or an implicit LUSGS scheme for the time integration [20]. For dynamic simulations a dual time-stepping method is employed, where on the pseudo time line a multi-grid cycle is used for convergence acceleration.

3. FLUID STRUCTURE COUPLING

The coupling of aerodynamics and structural dynamics as well as flight mechanics is approached via so called *loose coupling*, i.e. the aerodynamic solver and structural dynamic solver integrate the governing equations in time separately. The common boundary conditions are exchanged in finite time intervals. During this process displacements and forces are exchanged between the CFD code and the structural solver by spatial interpolation.

3.1. Spatial coupling

An approximation of the displacement field on the aerodynamic surface x_a is obtained linearly as a weighted superposition of the structural deformations x_s using a *spline matrix* H:

$$x_a = Hx_s \tag{3.1}$$

The identical spline matrix is used to transfer the aerodynamic forces f_a back into structural forces f_s:

$$f_s = H^T f_a \tag{3.2}$$

This plain approach is well known to ensure global energy conservation. The coefficients in H are preferably chosen applying radial basis functions (RBF). In addition, the spline matrix is formed in such a way, that on the one hand rigid body translations are reconstructed exactly and on the other hand the global balance of forces and moments is preserved during the load transfer [1][3][4]. Experience shows, that the proper choice of H poses a trade-off between accurate displacement interpolation and accurate force interpolation, i.e. a perfectly looking transfer of a typical large scale test deformation from the structural nodes to the aerodynamic surface might in turn lead to a locally ill distribution of aerodynamic forces on the structural nodes. The optimal RBF for each specific test case is selected by inspection of its behaviour on a dominant structural mode shape as well as vice versa for a load distribution on the undeformed wet surface [2].

Historically, two coupling strategies evolved called in the following *discrete approach* and *modal approach*. They differ in the handling of the degrees of freedom of the system: Either the orginal DOFs of the structural model are used in a straightforward manner or the system is described by a reduced basis of modal coordinates.

Discrete approach

Within this approach, complete system matrices M for the masses and K for the stiffnesses of the structural model are used. The matrices are obtained from MSC.NASTRAN. However, these matrices and hence the DOFs of the coupled system are condensed to the translatory degrees of freedom on the surface.

Neglecting structural damping, the linearised structural equations of motion read with eqn. 3.2 as

$$\begin{aligned} M\ddot{x}_s + Kx_s &= f_s \\ &= H^T f_a \end{aligned} \tag{3.3}$$

i.e. the aerodynamic forces are transferred back explicitly to the structural nodes every time step.

Modal approach

In this approach the structural elasticity is introduced from a modal decomposition of the discrete finite element model, thus leading to a linearly approximated elastic model which is based on a reduced number of modal degrees of freedom. With the mass-orthogonally scaled modal basis Φ_s and the generalized coordinates q

$$x_s = \Phi_s q$$

eqn. 3.3 can be written as

$$\begin{aligned}\ddot{q}+\Omega q &= \Phi_s^T f_s \\ &= \Phi_s^T H^T f_a \\ &= \left(H\Phi_s\right)^T f_a \\ &= \Phi_a^T f_a\end{aligned} \tag{3.4}$$

where the eigenvalues occur in the modal stiffness matrix $\Omega = \mathrm{diag}\left(\omega_1^2,\ldots,\omega_n^2\right)$. The right hand side of eqn. 3.4 shows the equivalence of the explicit back transfer of the aerodynamic forces and a following projection onto the structural eigenmodes to the direct projection of aerodynamic forces onto the individual mode shapes on the aerodynamic surface. The deformation of the aerodynamic surface is subsequently determined by

$$x_a = \Phi_a q$$

A reasonable number of structural modes has to be chosen to represent the dynamic and static behaviour appropriately. The structural eigenmodes have to be interpolated to the aerodynamic mesh only once during a preprocessing step. Favorably, this procedure allows convenient handling of free-free structures, since the aerodynamic forces can be easily split into forces working on rigid-body motion and forces working on elastic deformation. Additionally, the reduction to low wave number modes filters out local errors in the spatial interpolation. Contrarily to the discrete approach this method is inherently limited to linear structures.

3.2. Temporal coupling

In case of an unsteady aeroelastic fluid-structure simulation the time coupling scheme is usually based on a *Conventional Serial Staggered* algorithm (CSS) [6] modified with a predictor-corrector step for the structural displacements. In figure 0 the algorithm is depicted.

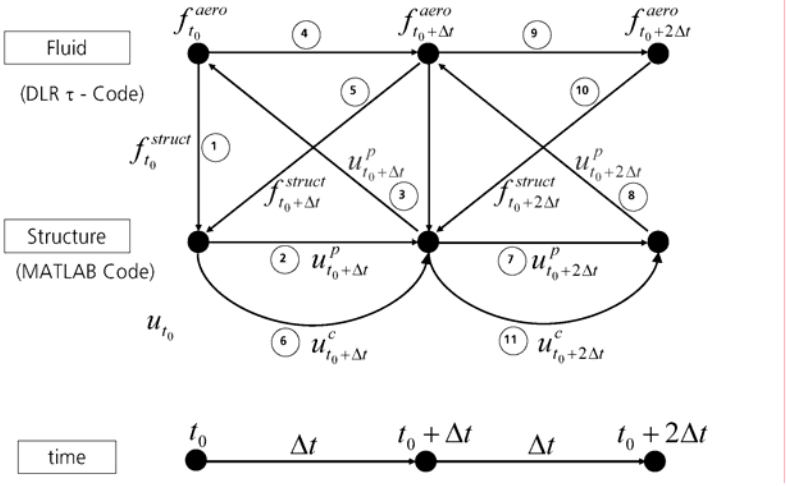

Figure 0: Conventional serial staggered algorithm with structural predictor/corrector

For the numerical verification of the coupled procedures, validated FE models of the test configurations AMP wing [11], HIRENASD wing [13], and A340-300 aircraft [12] are available. For the two dimensional NLR7301 airfoil the structural properties of the two degrees of freedom pitch and heave have

been measured [14], [15].

4. AMP WING WINDTUNNEL MODEL

A clean wing model has been considered for the current numerical investigation. A finite element (FE) structural model was designed that matches the frequencies and the mode shapes of the real model. Especially the bending and twist that have most influence on the flutter boundary. Table 1 displays the computed frequencies and the generalized mass compared to the measured data. The first mode shape of this model is shown in figure 1. Moreover, the computed mode shapes have been compared to the measured ones using Modal Assurance Criterion. The overall agreement between the FE model and the real model is good (see figure 1 right hand side). The agreements of the relevant mode shapes are very good and lies approximately at 99,5 % for the important first two mode shapes.

AMP - Fluttermodell						
		Frequenzen		generalisierte Massen		Frequenz-
Nr.	Eigenform	FE-Modell	Messung	FE-Modell	Messung	abweichung
1	1. Biegung	23.67 Hz	23.39 Hz	0.57 kgm²	0.58 kgm²	1.20 %
2	1. Torsion	31.79 Hz	31.85 Hz	10.91 kgm²	10.92 kgm²	0.19 %
3	1. H.-Biegung	49.69 Hz	49.00 Hz	1.56 kgm²	1.63 kgm²	1.41 %
4	2. Biegung	58.39 Hz	54.99 Hz	0.87 kgm²	1.63 kgm²	6.18 %
5	Biegung Bremse	****	81.06 Hz	****	5.38 kgm²	****
6	3. Biegung	104.49 Hz	99.60 Hz	1.61 kgm²	5.11 kgm²	4.91 %

Table 1: Computed frequencies and generalized masses versus measured data

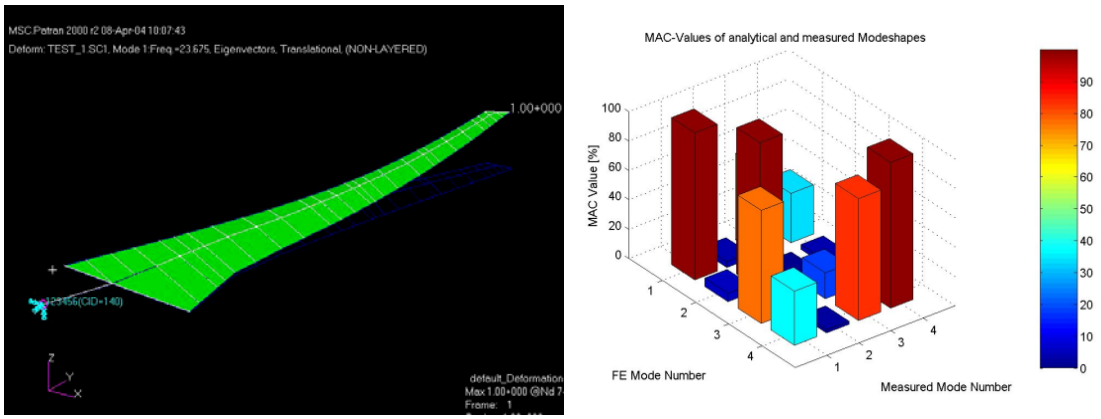

Figure 1: Bending of the AMP Wing at 23.67 Hz (left) and MAC values for the computed and measured mode shapes (right)

The selected test case is representative for transport aircraft cruise conditions, but with a 10 times smaller Reynolds number (due to the windtunnel test conditions) at transonic flow (Ma=0.82, α=2.55°, p0=0.9 bar, Re = 3.2 million). Viscous as well as inviscid computations were performed. The 1-equation Spalart-Allmaras turbulence model has been used for the viscous calculations. The unstructured mesh had 3,2 million elements and 1,0 million points, see figure 2.

Figure 3 shows that RANS computations are necessary to correctly predict the flow field and the structural deformation. The bending and twist deformations (Figure 4) are also much better predicted using RANS

simulations for the flow.

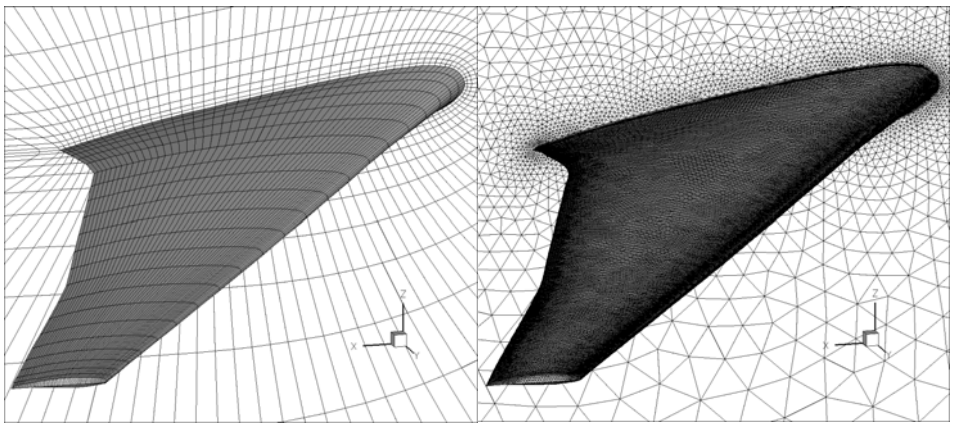

Figure 2: AMP grid used for Euler (left) and RANS (right) simulations

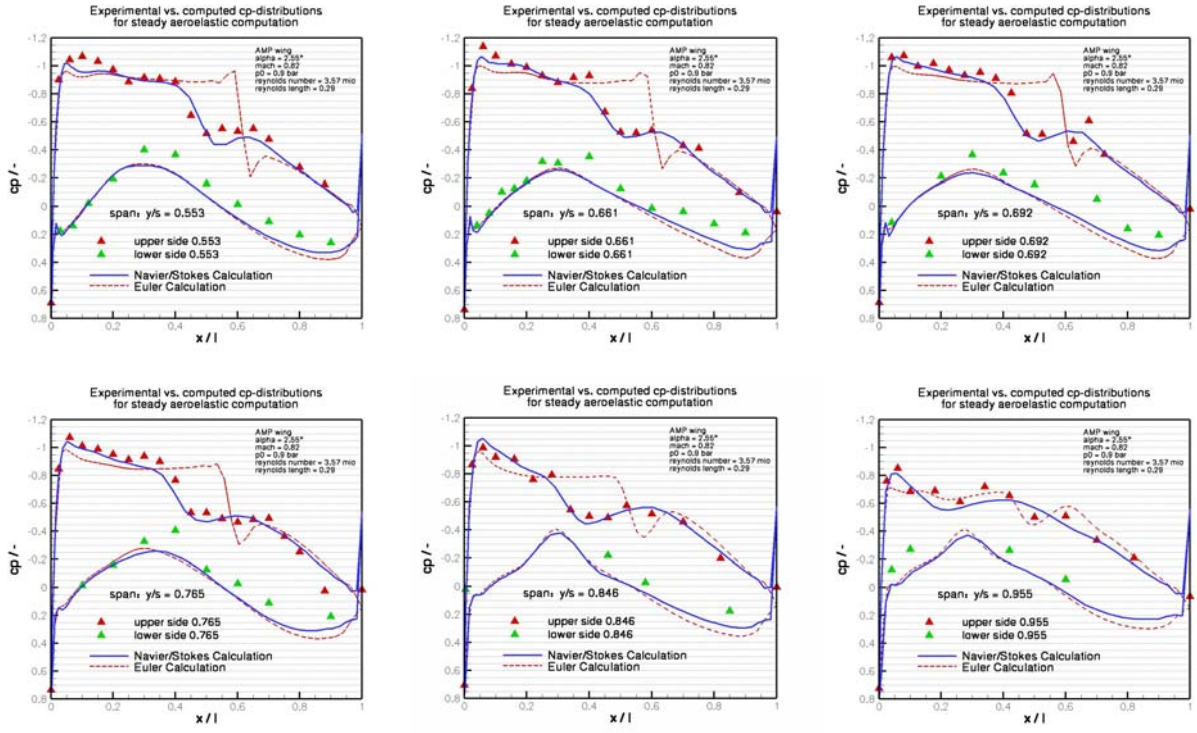

Figure 3: Cp distribution at respectively y=0.55/0.66/0.69 (top) and y=0.77/0.85/ 0.96 (bottom). Comparison between inviscid calculations (red line), viscous calculations (blue line) and experimental results (red and green triangles), Ma=0.82, a=2.55°, p0=0.9 bar

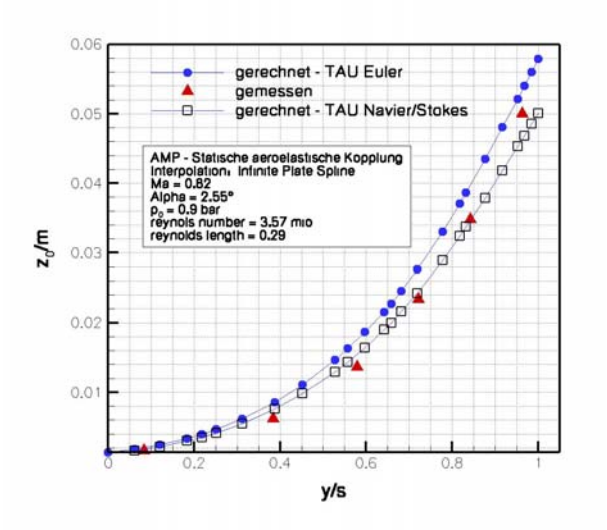

Figure 4: Comparison of the spanwise bending deformation for Euler (blue) vs. RANS (black), experimental data (red triangles) AMP wing Ma=0.82, a=2.55°, p0=0.9 bar

Flutter calculations were performed around the static equilibrium conditions at different Mach numbers by coupling unsteady RANS TAU Simulations (on the same CFD grid) with a NASTARN FEM model of 225 DOFs for the AMP wing. Figure 5 depicts the results together with the flutter boundary of other methods. Each symbol denotes the result of a single time domain simulation for specified values of Mach number and total pressure. Unstable, stable (damped) and limit cycle oscillations were observed, see figure 6. The boundary between stable and unstable behaviour agrees well with the flutter boundary in the wind tunnel tests. In addition also results from a classical p-k flutter analysis adopting generalized airloads from the classical doublet lattice method DLM and the fast linear transonic TDLM code [19] are depicted.

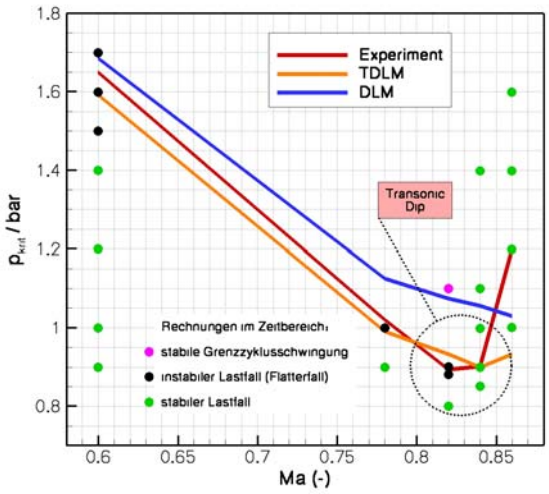

Figure 5: Numerical analysis of AMP stability boundary using different approaches, incl. time simulation

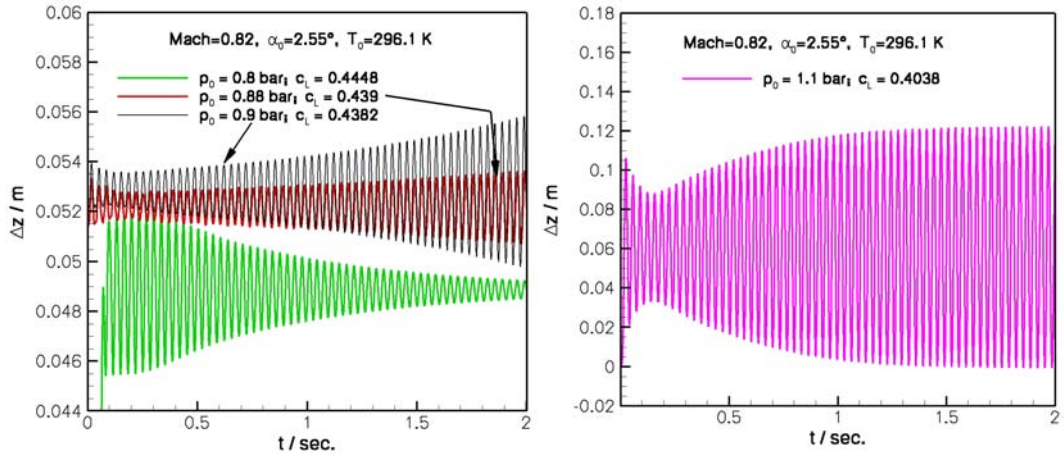

Figure 6: Time simulation of AMP-wing at stability boundary, Ma = 0.82

5. HIRENASD WIND TUNNEL MODEL

These tests have been carried out in 2006 at the European Transonic Windtunnel (ETW) under cryogenic conditions by RWTH Aachen together with DLR [13]. The objective of these tests was to create data base for static and dynamic aeroelastic code validation for a generic model of a transport aircraft at realistic Mach and Reynolds numbers, in contrast to the former AMP test. The static aeroelastic equilibrium conditions (AEC) for the HIRENASD wind tunnel model have been computed. A finite element model was used for the structural simulations. Whereas the original model, delivered by RWTH, had about 600.000 degrees of freedom and 250.000 nodes, the model used in the computations has been reduced significantly by taking only surface nodes into account.

Among others two different turbulence models (either 1-equation Spalart-Allmaras or 2-equation LEA-k-ω) and three different grids were tested and applied in coupling computations. As the influence of changing the turbulence model was small, the 1-equation Spalart-Allmaras model was used in most coupling computations. On the other hand the influence of the grids is significant. The three grids are a multi-block structured grid delivered by RWTH and two unstructured grids, which were generated by the Centaur software, one with sharp and one with blunt wing trailing edges, figure 7 depicts the blunt trailing edge grid. The grid with sharp trailing edge has significantly less points than the structured RWTH grid. The grid with the blunt trailing edge has the most points. The sizes of the grids are listed in table 2.

Navier-Stokes Grid	Number of nodes	Number of total cells	Number of surface cells
MB structured from RWTH	~ 3,26 Million	~ 3,18 Million	~ 160000
Unstructured sharp t.e.	~ 1,60 Million	~ 4,06 Million	~ 106000
Unstructured blunt t.e.	~ 5.37 Million	~ 14,18 Million	~ 311000

Table 2: Details respectively sizes of applied CFD grids

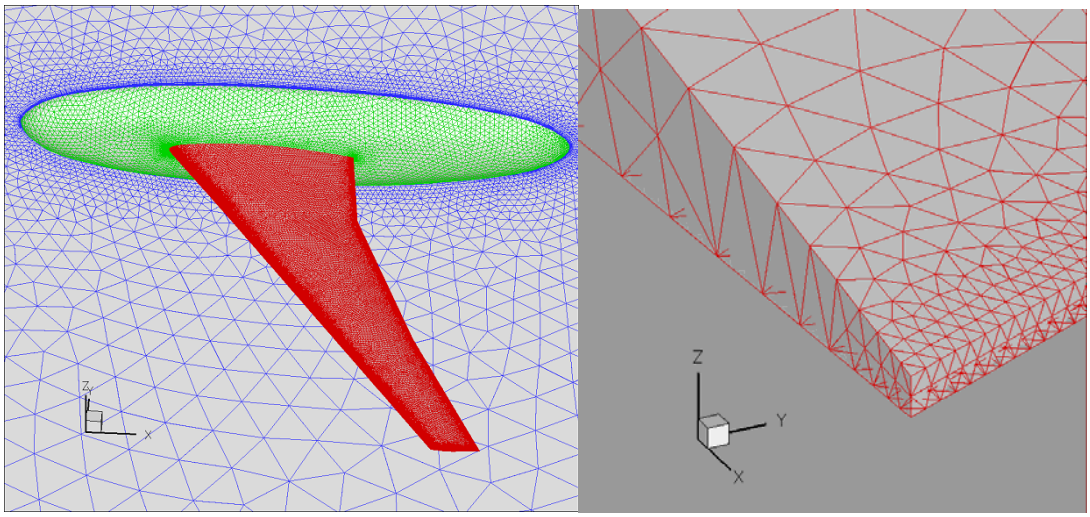

Figure 7: Unstructured grid for TAU RANS computations with blow-up of trailing edge

The computations were performed using Mach numbers of 0.70, 0.75, 0.80 and 0.88. This means a choice which covers the flow conditions subsonic, low transonic, transonic strong shock and transonic with shock induced separation. Since interesting transonic flow phenomena and significant wing deformation were found at a Mach number of 0.80 with a Reynolds number of 14*e+06 and a q/E ratio of 0.47*e-06, this case was investigated in more detail with various angles of attack (-1, 0, 1, 2, 3 degrees).

Results clearly indicate an increasing deformation of the model from fuselage to wing tip in spanwise direction, see comparison between Cp results for the jig shape and for the coupled solution at two wing sections in figure 8. From figure 8 it becomes clear that coupling the TAU code to the finite element model has a large influence on the resulting pressure distributions. We also observed that the numerical coupled calculations come very close to the results of the wind tunnel test, although not shown in this paper. Deformation also increases with the global wing load, which increases with angle of attack (AoA). This can be seen in figure 9, which shows the wing tip deflections.

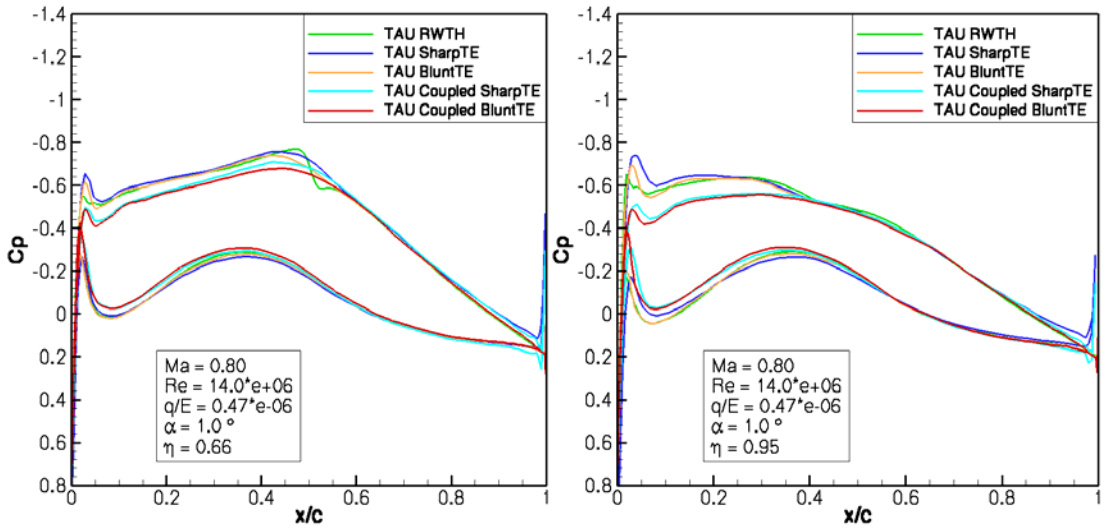

Figure 8: Computations of jig-shape versus aeroelastic equilibrium at inner section (66% span) and at wing tip (95% span) obtained on different CFD grids

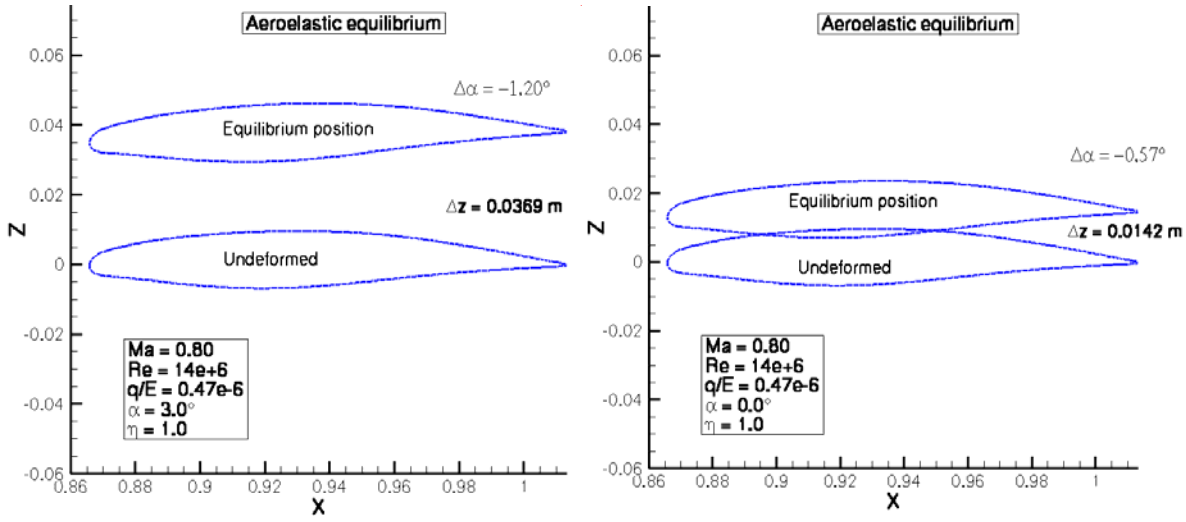

Figure 9: Wing tip deformation for two different load cases (AoA = 3 and 0 deg)

Figure 10 (left) demonstrates that the aeroelastic effect on pressure distribution for AoA = 3 degrees is much higher than for AoA = 1 degree in figure 10 (right). Fig. 10 (right) shows a comparison of jig shape with aeroelastic equilibrium simulations for different Reynolds numbers and different stagnation pressures q (Re = 7e+6, q/E = 0.22e-6 versus Re = 14e+6, q/E = 0.47e-6). The jig-shape ("standard") results show that the Reynolds number effect is small, while the aeroelastic simulations ("coupled") show the effect of stagnation pressure: increasing q yields an increase of loads and thus an increase of deformation and in turn a reduction of local angle of attack at the wing tip, followed by a local lift reduction.

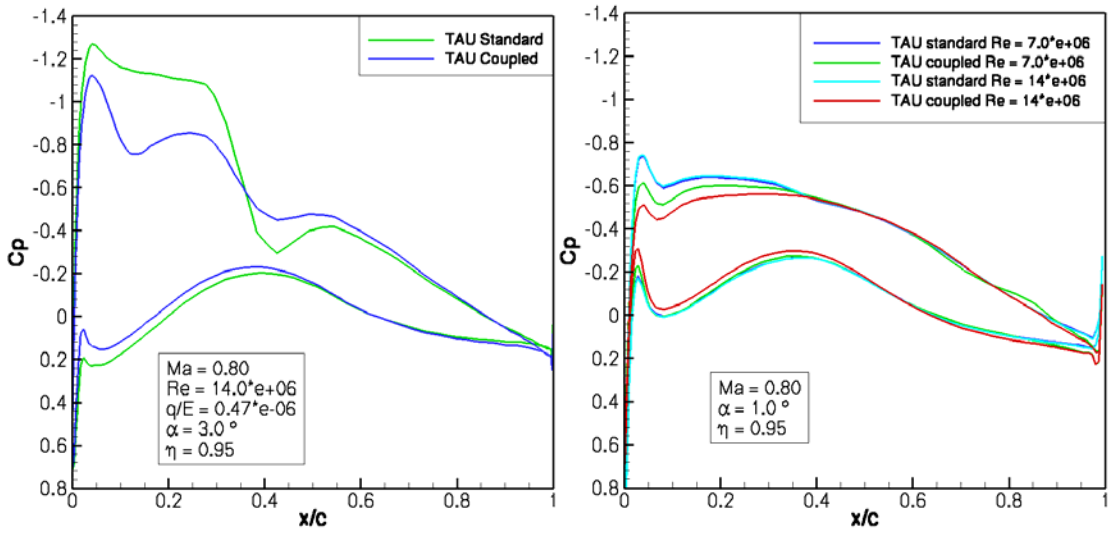

Figure 10: Left : Comparison of Cp for jig shape and elastically deformed wing (Ma=0.80, AoA = 3) Right : Influence of Re number and stagnation pressure q (Tau standard = jig shape, Tau coupled = aeroelastic equilibrium : Re=7 mio and q/E=0.22e-6 vs. Re=14 mio and q/E=0.47e-6)

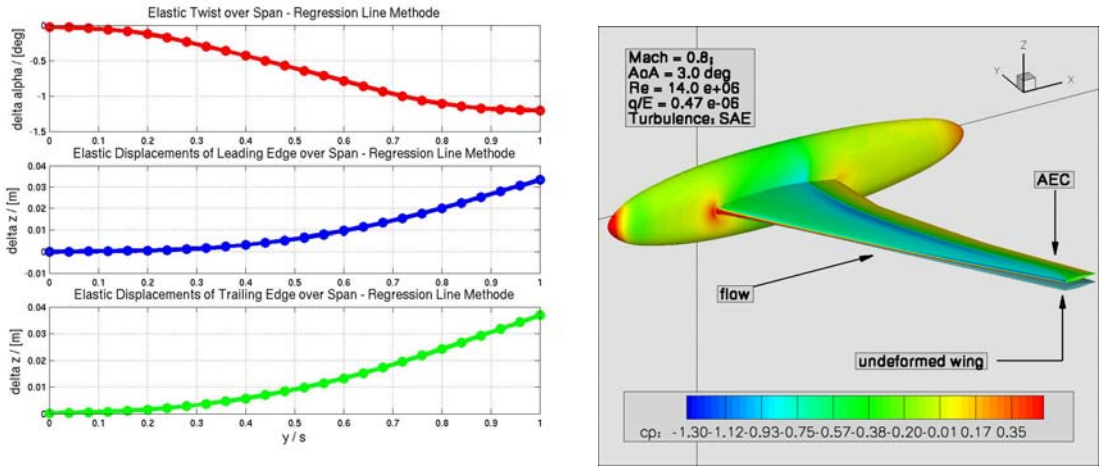

Figure 11: Deformation of leading and trailing edge and changes in AoA over wing span for case Ma=0.8, AoA=3.0 degree (left) and cp-distribution over fuselage and wing for AEC (right)

The dynamic aeroelastic behaviour of this configuration is simulated by disturbing the static equilibrium condition with an initial deflection of 15 mm at the wing tip. In spanwise direction the additionally applied deflection is decreasing proportional to the static aeroelastic deflection from jig shape. Figure 12 depicts the computed wing oscillation at the tip after releasing the system from the initial deflection at flow conditions: Ma=0.8, AoA = 2.0°, q/E = 0.47e-06. Two different calculations have been carried out. The first calculation was performed by using unsteady Euler aerodynamics and the second calculation has been accomplished with unsteady RANS aerodynamics. The results we obtained differ notably from one another. Especially the aerodynamic damping is much higher in the case of viscous calculation than with Euler aerodynamics. The dotted lines in figure 12 show the converged aeroelastic equilibrium for the Euler calculation (blue) and the RANS calculation (red). Furthermore the transient response shows a slight difference in the resonance frequency of the coupled system according to a higher damping. For the unsteady simulation we used a time step size of $\Delta t = 0.0005$ seconds.

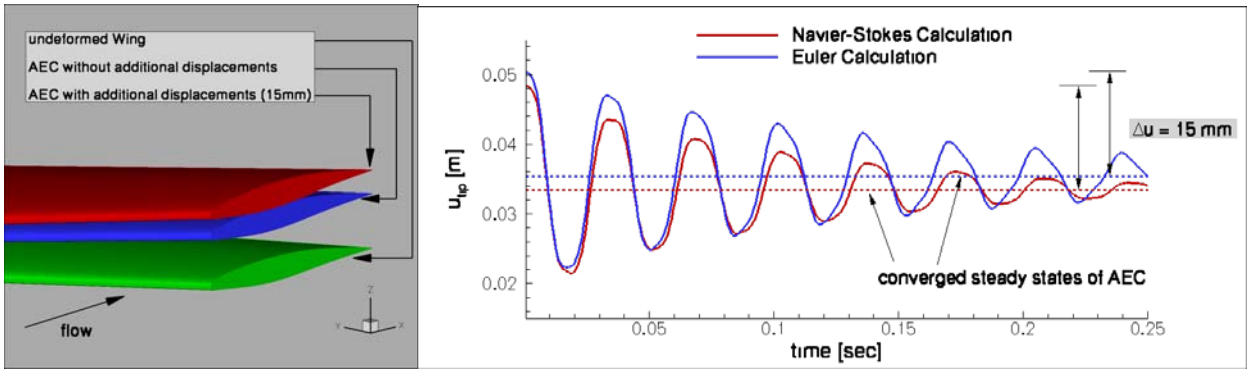

Figure 12: Dynamic aeroelastic simulation of a transient response with aerodynamic damped wing oscillation

6. A340-300 AIRCRAFT IN TRIMMED CRUISE CONDITION

Within the DLR project HighPerFlex (2004-2006) simulations for load alleviation by control surface deflection for a real aircraft have been performed including elasticity and trimming. The reference model

was an A340-300 passenger aircraft at cruise conditions.

The CFD grid comprises a half model with wing, fuselage, tails, winglets, control surfaces, pylons and flow-through engine nacelles, and has been generated by Centaur software as a hybrid grid with 10 million points, see figure 13 upper graphics.

The structural model comprises wings, winglets, control surfaces horizontal and vertical tails, as well as engine nacelles as MPCs. This model is available as MSC Nastran FE model with 200.000 degrees of freedom and is depicted in figure 13 in the lower graphics. A mass distribution of a total weight of 194 tons (with half filled fuel tanks) is applied for trim calculations. Trim condition was controlled for the elastic aircraft by control of balance between weight and lift and vanishing moment at the center of gravity. This was achieved by adapting the aircraft's global angle of attack and by deflection of the horizontal tail plane. The necessary angles were computed by a Newton iteration (see figure 16), where the Jacobian was obtained by straightforward finite differences. The angle of attack is introduced into the flow solver via modification of the farfield boundary condition, the tail deflection via grid deformation. The elastic deformations are computed with the modal method. The final shape is a superposition of the elastic deflections and the (small) control surface deflections.

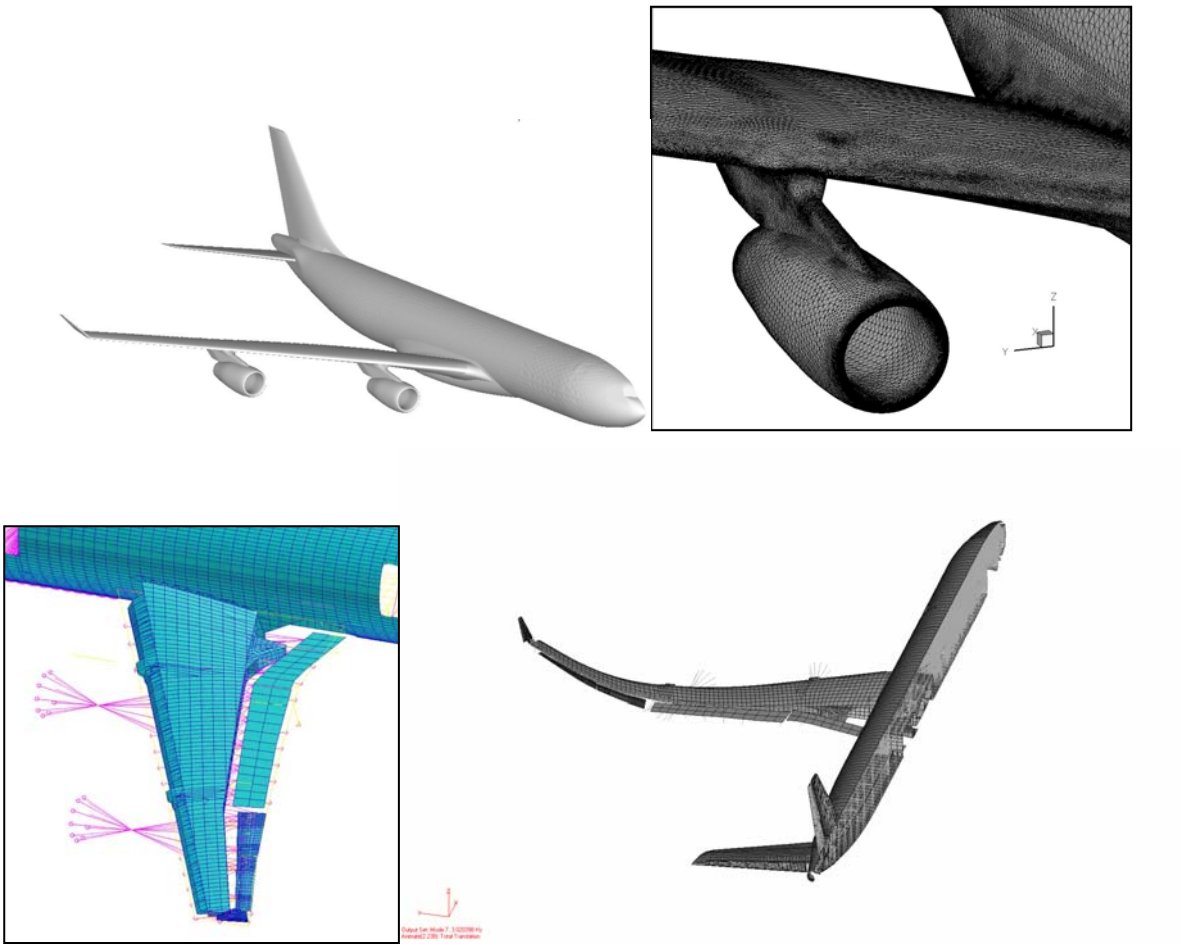

Figure 13: CFD and FE models of the A340-300 configuration

The advantages of the modal approach are:

- For the structure n eigenmodes and eigenvalues have to be computed only once (MSC Nastran

SOL 103)

- Only these eigenmodes have to be interpolated to the CFD surface.
- There is no need for an explicit back transfer of aerodynamic forces.
- Aerodynamic and inertia forces are split into rigid body and elastic forces. While rigid body forces do not have to be taken into account for the elastic deformations, they can be handled separately in the trim algorithm. Thus the aircraft can be modelled as free-free trimmed.
- Since for the interpolation of the mode shapes to the aerodynamic surface all FE-nodes can be used as control points no laborious selection of surface FE nodes is necessary.
- Usually a limited number of n = 20 – 200 eigenmodes are sufficient to achieve convergence in the elastic deformation.
- These first n eigenmodes are usually smooth, i.e. they have a long spatial wave length which improves the accuracy of interpolation.

The spatial interpolation of structural modal deflections to the CFD grid for a complete aircraft model often requires huge interpolation matrices. In the current A340 model more than 360.000 CFD surface grid points and 22.000 structural FE surface nodes are involved. For this reason the aircraft surface is split up into 200 partitions with mutual overlapping, and volume spline interpolation of the displacement field is performed for each partition separately. This yields an even local conservation of forces and moments while the sensitivity of the final result to the choice of the interpolating RBF is reduced.

Figure 14 shows the first and the second bending mode shape of the finite element model of the A340-300 in free vibration. The corresponding interpolated aerodynamic surface for the first mode shape is depicted in figure 15.

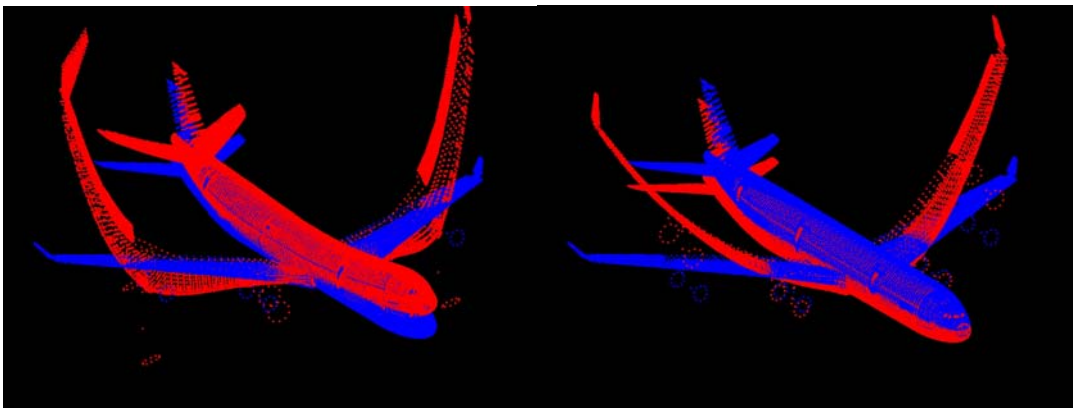

Figure 14: First and second bending mode shape of the finite element model

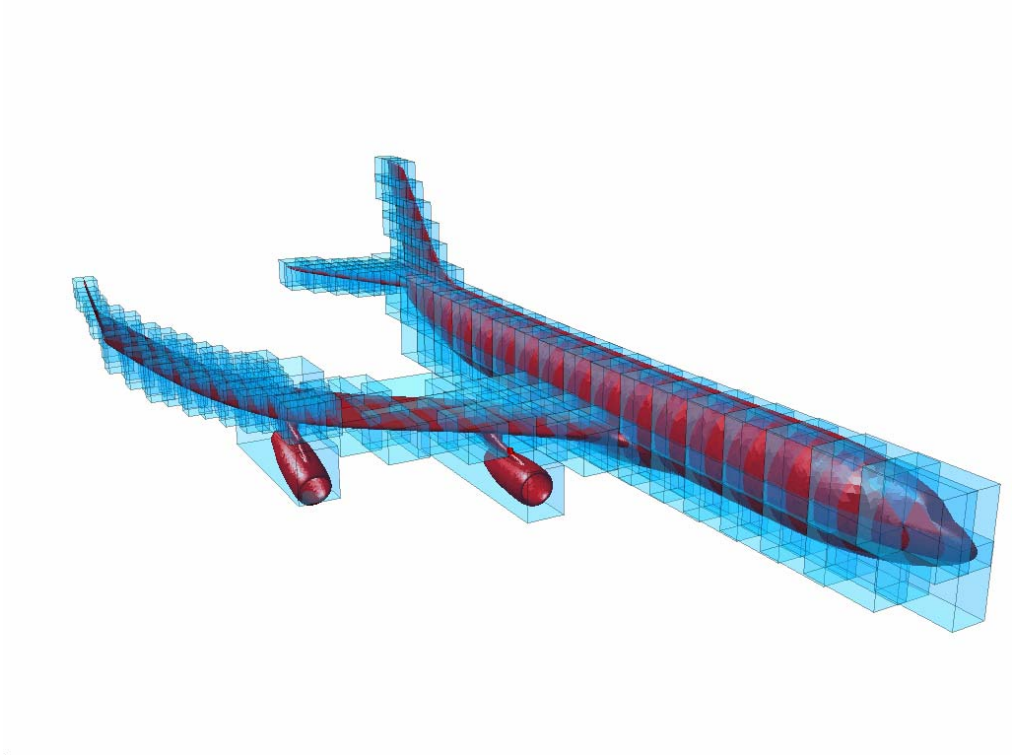

Figure 15: Partitioning of the model and interpolated aerodynamic surface for the first bending mode

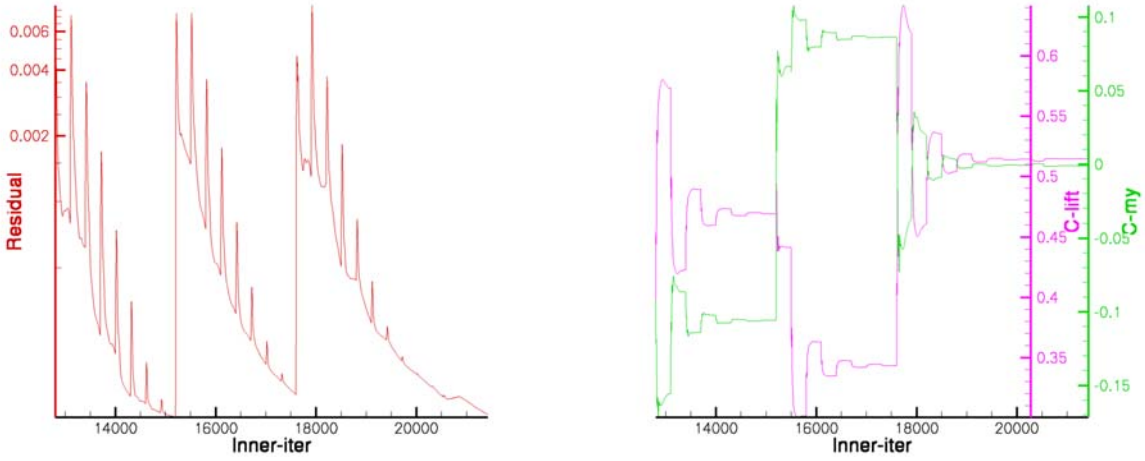

Figure 16: Convergence history during the trim loop. Lift is converging to 0.513, while the pitching moment around the centre of gravity is vanishing

7. TRANSONIC DIP AND LIMIT CYCLE OSCILLATIONS OF THE NLR7301 AIRFOIL

Wind tunnel data from DLR tests [14][15] for the supercritical NLR7301 airfoil are applied for assessment of unsteady aerodynamics in separated flow (buffet) and of fluid-structure coupling tools, for nonlinear

transonic flutter (LCO). The CFD grid for TAU RANS computations has 15150 prismatic cells in far field and 7488 structured prismatic cells in the boundary-layer region see figure 17 (right hand side). A sketch of the windtunnel model with 2 degrees of freedom (DOF), namely pitch and heave, is depicted in figure 17 (left hand side). For details about the model including structural parameters see [14][15].

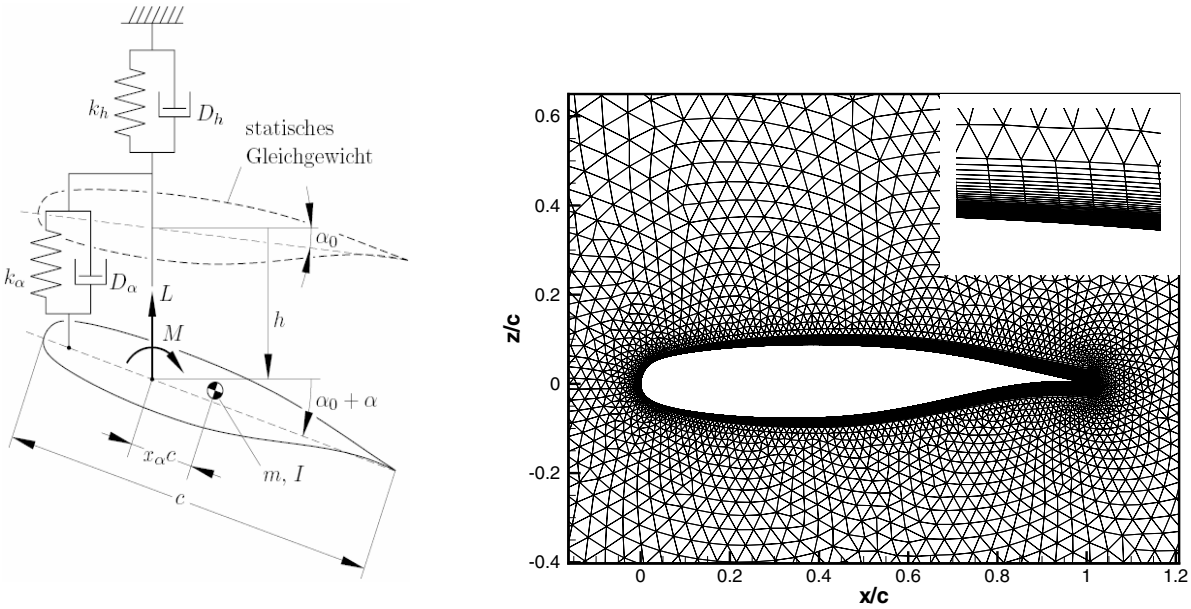

Figure 17: NLR7301 structure model (left) CFD grid for NLR7301 airfoil (right)

First flutter computations in the frequency domain have been performed in order to support a reference flutter boundary solution for the time domain flutter simulation, as well as to investigate the sensitivity to turbulence modelling. The computations were performed by using unsteady aerodynamic airloads, obtained by the TAU RANS code, adopting different turbulence models for forced harmonic oscillations in the pitch and heave degrees of freedom. About 100 URANS simulations for different mach numbers, reduced frequencies and the 2 DOFs were performed. For details see [16][17]. From these airloads the first harmonic linear unsteady components are extracted and used to form generalised airloads for the classical flutter computation by the p-k method. The flutter boundaries, obtained from this procedure are depicted in figure 18. The critical flutter index Fi is depicted as a function of mach number, while the static angle of attack was kept constant. Results show that:

- The flutter computations based on unsteady linear airloads determined by the TAU-code are able to provide the transonic dip for the supercritical NLR 7301 airfoil. For the Mach number of the minimum of the flutter boundary the airfoil encounters strong shocks.
- The transonic dip is more pronounced for the 2-equation turbulence model k-ω–LEA. The reason for this may be a different prediction of flow separation, see fig. 19. The 1 -equation model Spalart-Allmaras with Edwards modification (SAE) predicts a stronger shock induced separation also an onset of separation for a lower Mach number. Shock induced separation usually yields strong shift of phase of unsteady motion induced airloads, and this shift is responsible for a strong change of the flutter behaviour, which manifests here in a sudden rise of critical Fi. This happens with the SA turbulence model at a slightly lower (ΔMa = 0.01) Mach number value than with the LEA model.
- Unfortunately discrepancies between experiments and simulations are significant. One reasons for this may be that 3D and wall effects in the windtunnel experiments have not been accounted for in

the simulations.

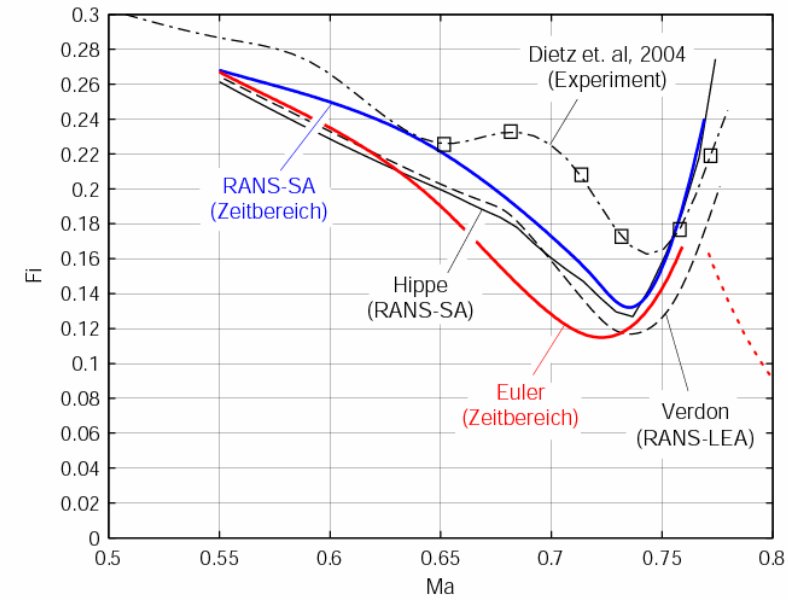

Figure 18: Measured and numerical predicted flutter boundary with different CFD methods. Results of classical fluter computations. The meanings of the labels are : Hippe (RANS SAE 1 equation turbulence model), Verdon (RANS k-ω LEA 2 equation turbulence model).

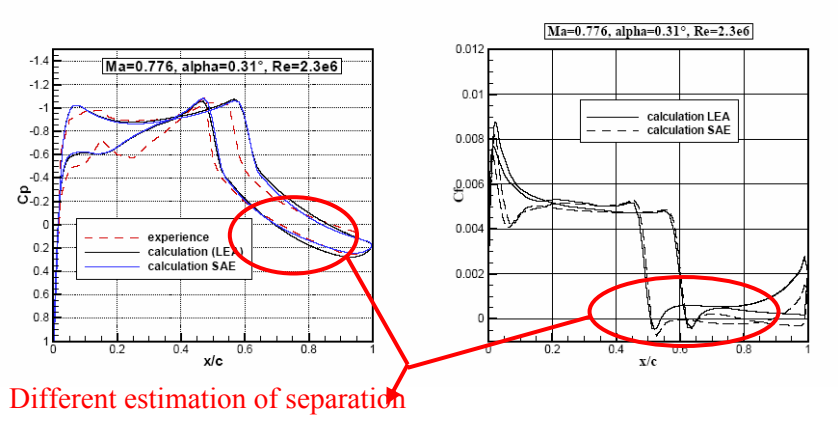

Figure 19: Influence of Turbulence Models on Steady Pressure Distribution and Skin Friction for a Mach number larger than at the minimum of the dip

Corresponding fluid structure coupled simulations in the time domain have been carried out adopting the TAU both in Euler and RANS modus with 1-equation turbulence model, [18]. Agreement with the frequency domain based results is good, see figure 18. Even with inviscid Euler aerodynamics a transonic dip is captured, but for lower Mach numbers, mainly due to Euler aerodynamics overpredicting shock strength.

Flutter with limited amplitude is a hard test case for nonlinear unsteady fluid structure interaction, because the mechanism of amplitude limitation is a nonlinear behaviour of either aerodynamic or structure. In these investigations only nonlinearity of aerodynamics is taken into account. It is well known that LCOs can originate even from inviscid aerodynamics, if significant shock motions are apparent [5], but for the

cases observed in the TWG for the NLR7301 airfoil viscous effects with and without flow separation seem to play an important role. Results of two LCO test cases are presented here and compared to the windtunnel results of [14] and [15]:

- MP 77, a test in the vicinity of shock induced flow separation, which is typical for the behaviour at higher Mach number dip with $\alpha = 1°$
- TL 3, a test case completely within the separation regime, which is typical for the behaviour at higher Mach number dip with $\alpha = 0°$

An overview of LCO results from simulations and experiments is listed in table 5:

case	Ma	Re [mio]	U [m/s]	ρ [kg /m^3]	μ	F_{index}	α_u	c_l	h_{LCO} [mm	α_{LCO} [°]	ω^*_F
MP77 test	0.768	1.7	256	0.383	954	0.204	1.28	0.272	0.75	0.2	0.242
MP77 sim.	0.754	1.7				0.200	-0.15			2.75	0.252
TL3 test	0.676	1.43	226	0.492	715	0.188	1.05	0.348	1.72	0.17	0.220
TL3 sim.	0.675	1.43			715	0.24	1.05				

Table 5: Test parameters and results for LCO test cases

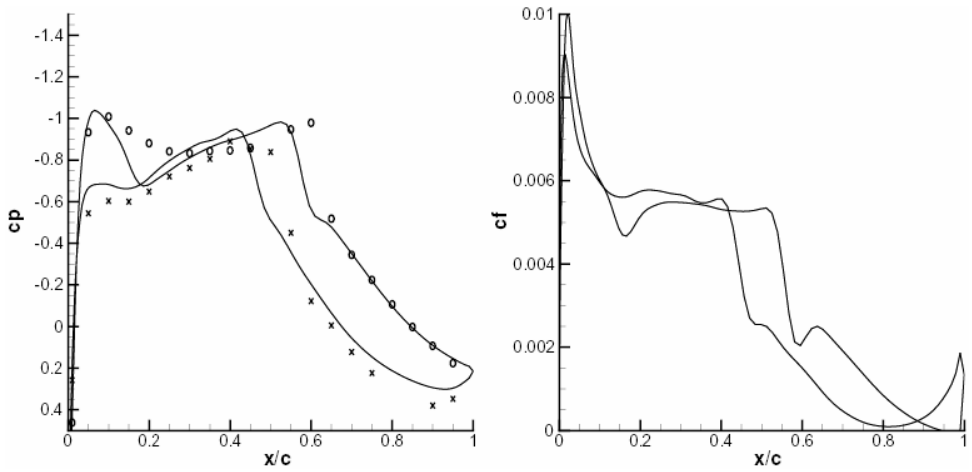

Figure 20: Steady pressure and skin friction distribution on airfoil for MP77 test case

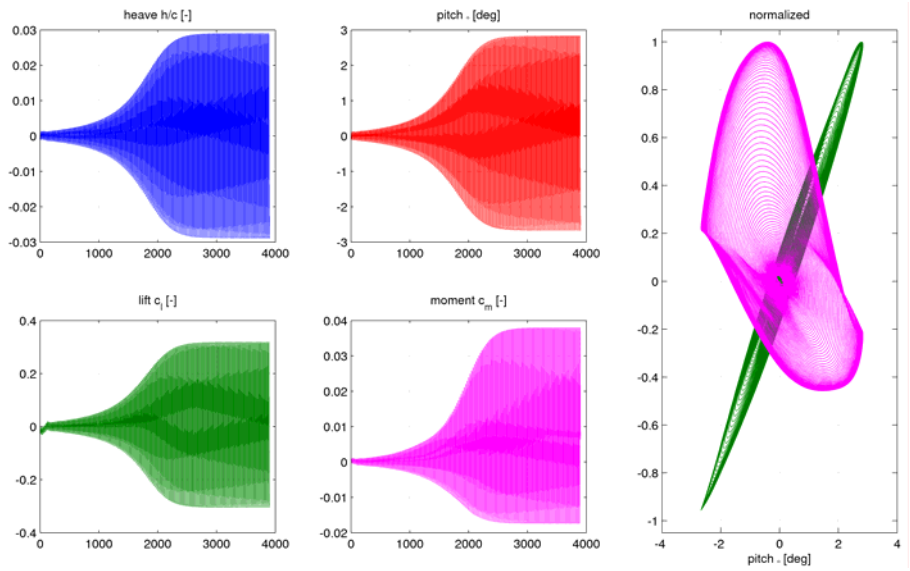

Figure 21: Time history of pitching and heaving motion

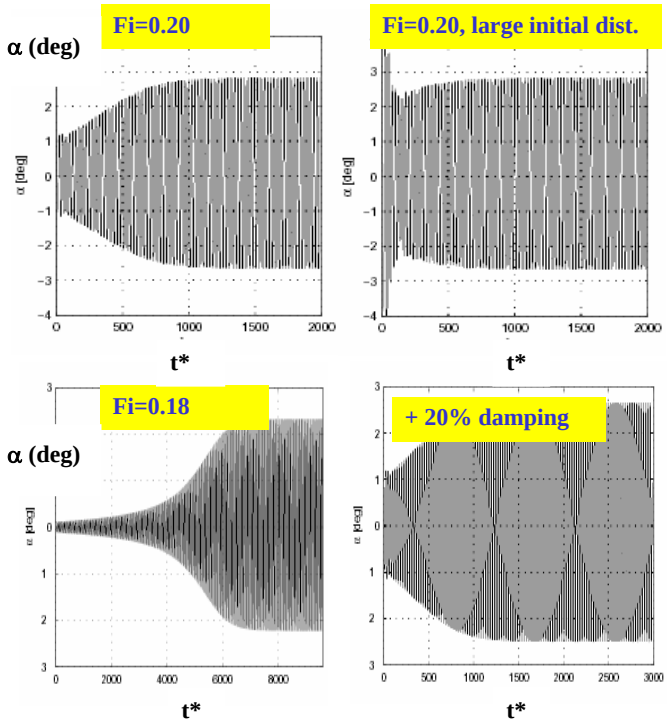

Figure 22: Influence of different parameters on the LCO amplitude.

Systematic flutter simulations in the time domain have been performed in order to capture LCO phenomena. Figure 21 depicts the steady pressure distribution corresponding to MP77, from TAU RANS computation with 1-equation SA turbulence model and from the tests (symbols). Best agreement with test results was obtained with changing the flow parameters Mach from 0.768 to 0.754 and α_{mean} from 1.28° to -0.15°, thus accounting for steady tunnel wall- and 3D effects. For these conditions the flow is not yet separated, as can be seen from the skin friction. Unsteady simulations in the time domain have been performed, integrating the 2 DOF structural model coupled with the TAU code. Figure 21, shows the

resulting time history of pitching and heaving motion, for lift and moment, starting from a very small disturbance of the steady state angle of attack. The simulation results in an exponential increase of amplitudes, followed by a transfer to limited constant amplitude values. These values are a factor 10 higher than those of the test, while the frequency values and ratio of amplitudes agree quite well. Figure 22 shows that the influences of small modifications of initial conditions, flutter index or structural damping are small.

An additional test case, which has been tested in the wind tunnel test section with adaptive and closed walls, and which exhibits nearly no flow separation, has been chosen. Due to the well defined tunnel wall conditions and to the lack in separation, this case should be better suited for validation than the MP77 case with perforated walls.

The flow parameters are: Mach = 0.6765, α = 1.51°, Re = 1.43 Million. Figure 23 depicts the steady flow surface pressure and LCO simulations for this test case for free flight conditions (without simulation of the walls). The LCO amplitudes are again much too large compared to the test results, namely $\Delta\alpha$ = 4.01° instead of 0.17° and Δh = 0.065 instead of 0.0027 chord, while again amplitude ratio and frequency are in good agreement.

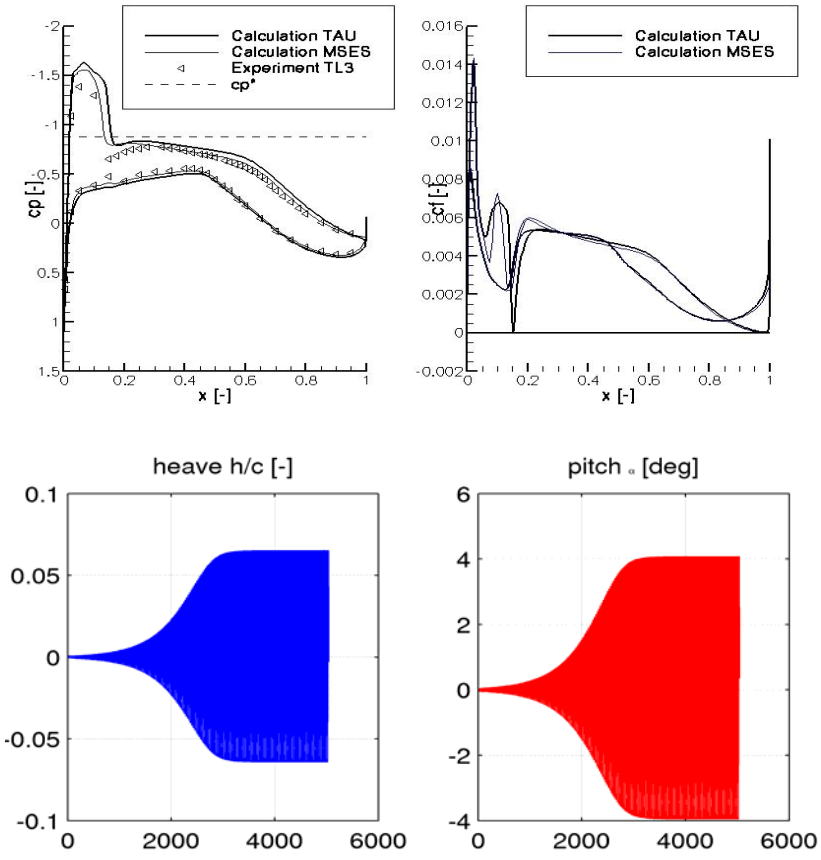

Figure 23: Numerical Simulations with TAU-code for LCO test case TL3

8. CONCLUSION

Numerical fluid structure coupling simulations have reached a certain amount of maturity in order to be applied both as reference results for classical aeroelastic simulation tools and as a necessary prediction

tool for transonic and separated flows. Static coupling has reached a high degree of reliability and has been validated for several test cases. Dynamic aeroelastic simulations in the time domain are often providing good results in prediction of transonic flutter boundaries, but are not yet validated for nonlinear flutter and limit cycle oscillations, especially in separated flow. This may have different reasons, namely a lack of reliable test results, too simplifying numerical assumptions about the windtunnel wall effects, neglect of nonlinear structural dynamic effects or non sufficient turbulence models. But even if quality of dynamic aeroelastic simulations can be further improved, the computational effort of time domain simulations remains high and is not acceptable for industrial aircraft flutter clearance. Here a reduction of computation time by a factor of 100 to 1000 is necessary. As the biggest part of computational effort is spent for CFD, such a reduction can only be achieved by development and application of unsteady aerodynamic models, which are derived from a significantly limited number of unsteady CFD calculations. These models can be used instead of DLM based aerodynamics within classical flutter calculations. This has been demonstrated in chapter 7 for the flutter boundary of the 2D airfoil. But even this approach is too time consuming for treating complex 3D structures with much more than 2 elastic modes. Further reductions of computational effort are promised by simplified unsteady aerodynamic methods, adopting either Euler-boundary layer coupling or time-linearised CFD. These methods have shown to be appropriate at least as long as no severe flow separation occurs. Use of the linearised TDLM unsteady aerodynamic method has been a first step and will be improved by linearised URANS codes. A second strategy may be application of Reduced Order Methods (ROM) or of correction methods for generalised airloads or Aerodynamic Influence Coefficient (AIC) matrices. These methods can be based on a limited number of well selected linear or nonlinear unsteady CFD simulations. This strategy will provide reasonable methods to achieve reliable results for flutter boundaries in transonic flow, even for mild flow separation, as long as small geometrical disturbances of the structural boundaries will result in small disturbances of the flow. For nonlinear flutter and flows with strong separation application of fluid structure coupling simulation in the time domain will probably remain necessary.

9. REFERENCES

[1] Beckert, A.; Wendland, H.: Multivariate Interpolation for Fluid-Structure-Interaction Problems using Radial Basis Functions. Aerospace Science and Technology, Art. No. 5125, 2001.

[2] Neumann, J.: Identifikation radialer Basisfunktionen zur räumlichen Strömungs-Struktur-Kopplung unter Berücksichtigung des Interpolations- und des Lasttransformationsfehlers. DLR-IB, IB 232-2008-J01, Deutsches Zentrum für Luft- und Raumfahrt, Göttingen 2008.

[3] Neumann, J.: Einarsson, G.Ó.; Schütte, A.: Multidisziplinäre Simulation eines rollenden, generischen Deltaflügels - Kopplung von Aerodynamik, Flugmechanik und Strukturdynamik. In: Proceedings, Deutscher Luft- und Raumfahrtkongress 2005, Friedrichshafen, 26.-29. September 2005.

[4] Neumann, J., Arnold, J., Krüger, W. R.: "Numerische Simulation komplexer aeroelastischer Phänomene und Vergleich mit Windkanalexperimenten", Proceedings of DGLR Annual Conference, Braunschweig, Germany, 2006.

[5] Schulze, S.: Transonic aeroelastic simulation of a flexible wing section. In : Numerical Unsteady Aerodynamic and Aeroelastic Simulation, AGARD Report 822, 10-1 – 10-20.

[6] Farhat, C., Lesoinne, M.: "Higher-Order Staggered and Subiteration Free Algorithms for Coupled Dynamic Aeroelasticitiy Problems, AIAA 98-0516, 1998.

[7] Gerhold, T.; Neumann, J.: The parallel mesh deformation of the DLR TAU-Code. 15. DGLR-Fach-

Symposium der STAB, Darmstadt (Germany), 2006-11-29-2006-12-01.

[8] Gerhold, T., Galle, M., Friedrich, O., Evans, J.: Calculation of Complex Three-Dimensional Configurations Employing the DLR-TAU Code. AIAA Paper 97-0167 (1997).

[9] Schwamborn, D., Gerhold, T., Heinrich, R.: The DLR-TAU Code: Recent Applications in Research and Industry. Proceedings of the European Conference on Computational Fluid Dynamics – ECCOMAS CFD 2006, Nordwijk, The Netherlands (2006). Available at : http://proceedings.fyper.com/eccomascfd2006/documents/619.pdf.

[10] CentaurSoft, CENTAUR, http://www.centaursoft.com.

[11] Zingel, H.: Measurement of steady and unsteady airloads on a stiffness scaled model of modern transport aircraft wing. Proc. Int. Forum on Aeroelasticity and Structural Dynamics, DGLR 91-06, pp.120-131 (1991).

[12] Henke, R.: Measurement of steady and unsteady airloads on a stiffness scaled model of modern transport aircraft wing. Proc. Int. Forum on Aeroelasticity and Structural Dynamics, DGLR 9

[13] Ballmann, J.: Measurement of steady and unsteady airloads on a stiffness scaled model of modern transport aircraft wing. Proc. Int. Forum on Aeroelasticity and Structural Dynamics, DGLR 9

[14] Schewe, G., Mai, H., Dietz, G.: Nonlinear effects in transonic flutter with emphasis on manifestation of limit cycle oscillations. Journal of Fluids and Structures 18 (2003), 3-22.

[15] Dietz, G., Schewe, G., Mai, H.: Amplification and amplitude limitation of heave/pitch limit cycle oscillations close to the transonic dip. Journal of Fluids and Structures 22 (2006), 505-527.

[16] Voß, R., Hippe, C.: Computation of the flutter boundary of the NLR7301 airfoil in the transonic range. Notes on Numerical Fluid Mechanics and Multidisciplinary Design Vol. 92 : New results in numerical and experimental fluid mechanics V. Springer 2005, 338-347.

[17] Verdon, N.: Computation of the flutter boundary of a transonic airfoil. Master thesis ENSIETA and DLR (2004)

[18] Nitzsche, J.: Simulation des transsonischen Flatterns eines Tragflügelmodells im Zeitbereich. Master Thesis TFH Berlin and DLR (2005).

[19] Lu, S., Voß, R.: TDLM - A Transonic Doublet Lattice Method for 3-D Potential Unsteady Transonic Flow Calculation and its Application to Transonic Flutter Prediction., Proc. International Forum on Aeroelasticity and Structural Dynamics 1993, 77-95.

[20] Dwight, R. P.,: Efficiency improvements of RANS-based analysis and optimization using implicit and adjoint methods on unstructured grids. PhD thesis Univ. of Manchester (2006).